Ultrasonic study of liquid crystals*

K. Miyano† and J. B. Ketterson
Department of Physics, Northwestern University, Evanston, Illinois 60201
and Argonne National Laboratory, Argonne, Illinois 60439
(Received 9 December 1974)

The ultrasonic velocity and attenuation in magnetically aligned liquid crystals has been measured. All well-known liquid-crystalline symmetries (nematic, cholesteric, and smectic *A*, *B*, and *C*) were studied. Sound anisotropy measurements in the smectic-*B* and -*C* and cholesteric materials are reported here for the first time; the measurements in the smectic-*C* and cholesteric liquid crystals are still in a preliminary stage. We unambiguously attributed the sound velocity anisotropy to the existence of a repeated structure (broken translational symmetry) in the hydrodynamic (low-frequency) limit by measuring the anisotropy across the nematic–smectic-*A* transition in *N*-*p*-cyanobenzylidene-*p*-octyloxyaniline (CBOOA); a sudden increase of the anisotropy extrapolated to zero frequency was observed at the transition despite a large dispersion. The smectic-*A*–smectic-*B* transition in ethyl-*p*-[(*p*-methoxybenzylidene)amino] cinnamate shows a two-dimensional liquid-to-solid transition. A distinct minimum was found at the nematic–smectic-*C* transition in *p*-*p*′heptyloxyazoxybenzene which was not accompanied by an attenuation peak. The velocity anisotropy in a cholesteric mixture of cholesteryl chloride and cholesteryl myristate was tentatively assigned to the dispersion.

I. INTRODUCTION

Many fluid-mechanical theories have been proposed for liquid crystals. In the early stages[1] the interest was mainly directed toward the mathematical aspects of the problem of generalizing conventional fluid mechanics to cover anisotropic fluids. Lately the problem has been considered in a wider framework[2–5]; e.g., to treat liquid crystals on the same basis as superfluids or binary liquid mixtures (as having additional internal degrees of freedom over normal fluids) and to note[6] the similarities between the normal to superconducting transition and the nematic–smectic-*A* transition.

Most of the theoretical work has been limited to the nematic case. Various points of view have arisen on how the theory should be constructed and there are even differences in the final expressions for the dynamics of the nematics. The differences occur over the existence of terms with a microscopic character. The relevancy of such terms is debatable. However, it turns out that these terms are of higher order in the frequency ω and the wave vector $\vec{q}$ and, in the hydrodynamic limit $(\omega, q \to 0)$, all theories agree. A conclusion is that there is no sound velocity anisotropy in the nematics. For the smectic and cholesteric liquid crystals, theories predict a velocity anisotropy and its form. A systematic analysis[2,4] shows that the sound velocity anisotropy can be traced back to the existence of a repeated structure in the liquid crystals. One can argue this in terms of the breaking of translational symmetry. An additional hydrodynamic mode introduced by this "symmetry breaking" brings about the anisotropy of the longitudinal sound velocity. On the other hand, microscopically one can argue that a stress gradient is supported by the very molecular forces that make the repeated arrangement more stable than a random one. Due to the fact that the structure can support a stress gradient, the uniaxial compressibility is not isotropic and hence an anisotropic sound velocity occurs. In any event, the arguments are valid only in the hydrodynamic limit. As a low-frequency probe, ultrasound is well suited to test the above theories.

Extensive ultrasonic experiments[7] have been performed in aligned nematic liquid crystals; some studies[8,9] in the aligned smectic-*A* materials have appeared. In other liquid-crystalline symmetries, sound experiments were done only in nonaligned samples and thus the anisotropic features were obscured. We present here a series of ultrasonic experiments in magnetically aligned liquid crystals, and we relate the sound anisotropy to the liquid-crystal symmetry.

Phase transitions between various mesophases, other than the isotropic–nematic (I-N) and the nematic–smectic-*A* (N-A) transitions, have not been well studied. We draw attention to some of these transitions as offering great potential for future study.

In Sec. II we briefly discuss the theoretical background and the phenomenological formalism used to analyze the data. Section III deals with the experimental techniques and in Sec. IV we present the experimental data and their interpretations. To maintain an orderly presentation we discuss each material separately.

II. DATA ANALYSIS AND THEORY

A. Phenomenological description

When one considers the *linearized* equations of motion for an isotropic solid and a simple fluid a strong resemblance between them is apparent. By introducing the transformations $\nabla_j \to iq_j$ and $\partial/\partial t \to -i\omega$ we note that the equation can in both cases be written as

$$F_i = iq_k[\bar{K}u_{ll}\delta_{ik} + 2\bar{\mu}(u_{ik} - \tfrac{1}{3}u_{ll}\delta_{ik})], \tag{1}$$

where (in a solid) F_i is the ith component of the force, $\bar{K} = K - i\omega\zeta$, where K is the bulk modulus and ζ is the bulk viscosity, $\bar{\mu} = \mu - i\omega\eta$, where μ is the shear modulus and η is the shear viscosity, and $u_{ij} = \frac{1}{2}(\nabla_i u_j + \nabla_j u_i)$, where u_i is the ith component of the displacement vector and ∇_i is the derivative with respect to the ith spatial coordinate. It is understood that in a normal fluid $1/K$ is the compressibility and $\mu = 0$. Equation (1) thus parametrizes the equation of motion in an isotropic body, fluid or solid. A natural way to extend this approach to liquid crystals is to apply the equation of motion for anisotropic solids (crystals) to liquid crystals. We could write an equation similar to Eq. (1) by making $\bar{K}$ and $\bar{\mu}$ tensors of rank 4. However, in the traditional theory of elasticity it is customary to introduce elastic stiffness constants c_{ij} which relate the strain u_{ij} and the stress σ_{kl} as[10]

$$\sigma_{11} = c_{11}u_{11} + c_{12}u_{22} + c_{13}u_{33} + 2(c_{14}u_{23} + c_{15}u_{31} + c_{16}u_{12}), \tag{2}$$

$$\sigma_{22} = c_{21}u_{11} + \cdots .$$

If we choose the c_{ij} matrix appropriate to a hexagonal crystal, which also includes uniaxial symmetry as a special case, the matrix is suitable to describe the symmetry of the nematic, smectic-A, and smectic-B liquid crystals. There are five independent nonzero elements in the matrix for a hexagonal crystal: $c_{11} = c_{22}$, c_{12}, $c_{13} = c_{23}$, c_{33}, $c_{44} = c_{55}$, and $c_{66} = \frac{1}{2}(c_{11} - c_{12})$. As will be shown later, as far as the sound velocity is concerned, the symmetry of the smectic-C and cholesteric phases is also expressed by the same c_{ij} matrix.

We make the following substitutions[11]:

$$c_{ij}/\rho \to \bar{C}_{ij} = C_{ij} - i\omega D_{ij}. \tag{3}$$

The complex sound velocity $\bar{V}$ ($\bar{V} = V - i\omega V'$), for the mode which is a pure longitudinal wave for propagation along a symmetry axis and is dominantly longitudinal for off-axis propagation, is then given by

$$2(\bar{V})^2 = \bar{C}_{11}\sin^2\theta + \bar{C}_{33}\cos^2\theta + \bar{C}_{44} + \{[(\bar{C}_{11} - \bar{C}_{44})\sin^2\theta - (\bar{C}_{33} - \bar{C}_{44})\cos^2\theta]^2 + 4(\bar{C}_{13} + \bar{C}_{44})^2\sin^2\theta\cos^2\theta\}^{1/2}, \tag{4}$$

where θ is measured from the 3-axis.

For the sound wave to be a well-defined mode it must propagate many wavelengths without an excessive attenuation. This requires that $V \gg \omega V'$ or, equivalently, $C_{ij} \gg \omega D_{kl}$. Under this condition the attenuation coefficient α is written as

$$\alpha = \omega^2 V'/V^2. \tag{5}$$

If we further assume that the velocity anisotropy is small (which is usually the case) the velocity V and the attenuation coefficient α are easily obtained as

$$2V^2 = C_{11}\sin^2\theta + C_{33}\cos^2\theta + C_{44} + \{[(C_{11} - C_{44})\sin^2\theta - (C_{33} - C_{44})\cos^2\theta]^2 + 4(C_{13} + C_{44})^2\sin^2\theta\cos^2\theta\}^{1/2}, \tag{6}$$

$$\alpha = (\omega^2/2V^3)[D_{11}\sin^2\theta + D_{33}\cos^2\theta + (2D_{13} + 4D_{44} - D_{11} - D_{33})\sin^2\theta\cos^2\theta], \tag{7}$$

where only the first order in $\omega D_{ij}/C_{kl}$ was retained. C_{44} is the shear component in the 1-3 and 2-3 planes; if the smectic planes can glide freely over each other C_{44} must be zero. Equations (6) and (7) are the main results which we used to analyze our data. The sound velocity and attenuation were measured as a function of the angle θ; the parameters C and D were determined by the least-squares method.

B. Dispersion

In some cases C and D are frequency dependent. This is usually manifested as a frequency dependence of α/ω^2; this ratio should be frequency independent in the absence of dispersion.

In an isotropic fluid the ratio between the local pressure and density change produced by the sound wave, $\partial p/\partial\rho$, is not necessarily constant because of the possible existence of a slow internal relaxation process. The thermodynamic derivative $\partial p/\partial\rho$ then has the frequency-dependent form[12]

$$\frac{\partial p}{\partial \rho} = \left[\left(\frac{\partial p}{\partial \rho}\right)_0 - i\omega\tau\left(\frac{\partial p}{\partial \rho}\right)_\infty\right]\Big/(1 - i\omega\tau), \tag{8}$$

where 0 and ∞ refer to zero and infinite frequency, respectively, and τ is the relaxation time associated with internal equilibrium.

In a liquid crystal there might be several (anisotropic) lifetimes. Let us assume for the simplicity that there is one relaxation process[13] in our fre-

quency range with a time constant τ. The parameters $\bar{C}_{ij}$ are presumed to have different zero- and infinite-frequency values and have a form similar to Eq. (8). We consider the differences $C_{33}(\omega^2) - C_{11}(\omega^2)$ and $D_{11}(\omega^2) - D_{33}(\omega^2)$; the argument is ω^2 because of the time-reversal symmetry. Then it is easily shown that

$$C_{33}(\omega^2) - C_{11}(\omega^2) = C_{33}(0) - C_{11}(0) + \frac{(\omega\tau)^2}{1+(\omega\tau)^2}\Delta, \tag{9}$$

$$D_{33}(\omega^2) - D_{11}(\omega^2) = \frac{\tau\Delta}{1+(\omega\tau)^2}, \tag{10}$$

where $\Delta = C_{33}(\infty) - C_{33}(0) - C_{11}(\infty) + C_{11}(0)$. The reason we have chosen these quantities is that they can be accurately measured. The above combinations involve both a volume change and a shear deformation. Later we shall also consider the dispersion of a combination $C_{11} + C_{33} - 2C_{13}$, which does not involve a volume change.

C. Theory

We use the hydrodynamic theory developed by Martin *et al.* Those who are interested in the details should refer to Ref. 4. The theory starts with the recognition of two origins for hydrodynamic modes (defined as modes that have a structure $\omega \to 0$ as $q \to 0$). One origin is the conservation laws, where a time variation of a generalized density is proportional to the divergence of a corresponding current. The other origin is broken symmetries or deformations in an ordered system.

What is unique in liquid crystals is the existence of such hydrodynamical modes due to the order. The problem is then to find the proper variables that describe the particular order in each liquid-crystal symmetry. Let us denote such variables by $\{x^\alpha\}$. By incorporating a form $\sum_\alpha \phi_i^\alpha \, d\nabla_i x^\alpha$ (ϕ^α is a "force field" conjugate to x^α) into the free energy of a simple fluid one can obtain the desired formalism for liquid crystals.[4] We only show the final results.

1. Nematics

In the nematics the new variable is the director $\vec{n}$. With the director initially parallel to the 3-axis, a small variation may be expressed as

$$\delta\dot{n}_i = \tfrac{1}{2}\lambda(\nabla_i v_3 + \nabla_3 v_i) - \tfrac{1}{2}(\nabla_i v_3 - \nabla_3 v_i), \quad i = 1,2 \tag{11}$$

where λ is a parameter. Let us note that in the hydrodynamics of a simple fluid the reactive part of the energy current density, for instance, is[12] $(p+\epsilon^0)v_i$ (p is the pressure and ϵ^0 the energy density of fluid at rest). Compared to this, Eq. (11) is one order higher in q. Therefore we can neglect the effect of the director on the reactive part of the hydrodynamic equations (sound velocity). Thus the necessary equations are

$$\begin{aligned} &\dot{\rho} + \rho\nabla_i v_i = 0, \\ &\dot{Q} = \dot{\epsilon} - \rho^{-1}(\epsilon + p)\dot{\rho} = \kappa_\perp(\nabla_1^2 + \nabla_2^2)T + \kappa_\parallel \nabla_3^2 T, \\ &\rho\dot{v}_i = -\nabla_i p + \eta_{ijkl}\nabla_j \nabla_l v_k, \end{aligned} \tag{12}$$

where $\kappa_\parallel$ and $\kappa_\perp$ are the thermal conductivity parallel and perpendicular to the director, respectively, and the η's are the viscosity coefficients pertinent to the uniaxial symmetry. There is no velocity anisotropy; $V = (\partial p/\partial\rho)_s^{1/2}$ [i.e., $C_{11} = C_{13} = C_{33} = (\partial p/\partial\rho)_s$]. The attenuation anisotropy is given by Eq. (7) with the substitutions

$$\begin{aligned} &\rho D_{11} = \eta_2 + \eta_4 + \kappa_\perp(\gamma - 1)/C_p, \\ &\rho D_{33} = \eta_1 + \kappa_\parallel(\gamma - 1)/C_p, \\ &\rho(2D_{13} + 4D_{44} - D_{11} - D_{33}) = 2\eta_5 + 4\eta_3 - \eta_1 - \eta_2 - \eta_4, \end{aligned}$$

where C_p is the specific heat at constant pressure, $\gamma = C_p/C_v$, and we have used the viscosity notation of Ref. 4.

2. Smectic-A

The variable x here is the deformation of the planes from the equilibrium position. We take the plane normal parallel to the 3-axis. The equations are then

$$\begin{aligned} &\dot{\rho} + \rho\nabla_i v_i = 0, \\ &\dot{x} - v_3 = \xi\nabla_i\phi_i + \xi T^{-1}\nabla_3 T, \\ &\dot{Q} = \xi\nabla_3\nabla_i\phi_i + \kappa_\perp(\nabla_1^2 + \nabla_2^2)T + \kappa_\parallel\nabla_3^2 T, \\ &\rho\dot{v}_i = -\nabla_i p + \delta_{13}\nabla_j\phi_j + \eta_{ijkl}\nabla_j\nabla_l v_k, \end{aligned} \tag{13}$$

where ζ is the diffusion constant and ξ is a coefficient which accounts for a coupling between the diffusion and the temperature gradient. The velocity anisotropy is readily calculated by neglecting all dissipative effects in Eq. (13). It is given by Eq. (6) with the substitutions

$$C_{11} = \left(\frac{\partial p}{\partial\rho}\right)_{sx},$$

$$C_{33} = \left(\frac{\partial p}{\partial\rho}\right)_{sx} - \frac{2}{\rho}\left(\frac{\partial p}{\partial\nabla_3 x}\right)_{s\rho} + \frac{1}{\rho}\left(\frac{\partial\phi_3}{\partial\nabla_3 x}\right)_{s\rho},$$

$$C_{13} = \left(\frac{\partial p}{\partial\rho}\right)_{sx} - \frac{1}{\rho}\left(\frac{\partial p}{\partial\nabla_3 x}\right)_{s\rho}.$$

The attenuation anisotropy is rather complicated and will be discussed in Appendix A.

3. Smectic-B

The smectic-B phase has order in the 1-2 plane. Therefore terms like $(\partial\phi_1^2/\partial\nabla_1 x_2)$ enter into the reactive part, where in this case the generalized displacement x^2 is identical to the real space coordinate x_2. This affects the C_{12} element in the notation of Sec. II A. The C_{44} element is of higher order in $\vec{q}$. Thus there are four independent nonzero elastic constants in this case compared with five for a general hexagonal crystal. Because the C_{12} element does not affect the longitudinal sound velocity [Eq. (6)] our data analysis procedure remains the same as before, except that C's contain more terms like $\partial\phi_2^2/\partial\nabla_2 x_2$.

4. Smectic-C

The difference between the smectic-A and smectic-C phases is that in the latter the molecules are not perpendicular to the planes. As was discussed in the case of the nematics, the effect of the molecular orientation on the reactive part is of higher order in $\vec{q}$ than that of other variables. Therefore as far as the sound velocity is concerned, the C matrix is the same as that for the smectic-A phase.

Thus the longitudinal sound velocity data of the smectic-B or -C phases were analyzed in the same way as those for the smectic-A. The attenuation in the smectic-B and -C phases is exceedingly complicated because of all the additional variables that come into play, and there is no *a priori* reason why one variable should have an order-of-magnitude smaller effect than another. Too many parameters are thus involved and the measurement of longitudinal sound is insufficient to reveal the full dissipative processes.

There are two thermodynamic stability conditions that a system must satisfy: The system should be at the minimum of the free energy and the entropy production must be positive. We call the former static stability and the latter dynamic stability.

In a simple isotropic system, static stability implies the well-known thermodynamical inequalities: $(\partial p/\partial\rho)_x > 0$ and $(\partial T/\partial s)_\rho > 0$ (the compressibility and the specific heat are always positive). In the smectic-A phase there are additional conditions:

$$\left(\frac{\partial\phi_3}{\partial\nabla_3 x}\right)_{s\rho} > 0,$$

$$\frac{1}{\rho}\left(\frac{\partial p}{\partial\rho}\right)_{sx}\left(\frac{\partial\phi_3}{\partial\nabla_3 x}\right)_{s\rho} - \left(\frac{\partial\phi_3}{\partial\rho}\right)_{sx}^2 > 0.$$

In terms of the C's these conditions are $C_{11} > 0$, $C_{33} + C_{11} - 2C_{13} > 0$, and $C_{11}C_{33} - (C_{13})^2 > 0$.

Similarly, dynamical stability demands that the matrices κ, η, etc., be positive definite. In a simple liquid this means that the thermal conductivity κ and the bulk and shear viscosities, ζ and η, are all positive. For the viscosity matrix for a uniaxial system the conditions are that η_1, η_2, η_3, $\eta_4 > 0$ and $\eta_1\eta_4 > \eta_5^2$.

III. EXPERIMENTAL TECHNIQUE

A. Ultrasonics

A phase-sensitive technique was used for accurate measurements. A block diagram of the experimental setup is shown in Fig. 1. A continuous radio-frequency (rf) source was split into two branches, a signal branch and a reference branch. Frequencies between 2 and 36 MHz were used. The rf in the signal branch was switched (to produce a pulse), amplified, and fed to a sonic cell. In the reference branch the rf was also switched (at the time of arrival of a signal from the sonic cell), applied to an attenuator and delay line, and finally combined with the signal pulse. The combined pulse was amplified, rectified, and displayed on a scope. The attenuation and delay time in the reference branch were adjusted so that the reference pulse canceled the signal pulse, the condition being a 180° phase difference and an equal amplitude for the two pulses. We have two external variables: the temperature and the magnetic field. For some initial values of these external variables, the attenuation and the delay time were marked; the changes necessary to restore the cancellation were then recorded as a function of the variables. This method yielded accurate values of the attenuation and velocity change *relative* to those of the initial values of the external variables. For instance, at 12 MHz it took ~5 μsec for a pulse to pass through a path length of 7.8 mm. The delay line employed could be varied in 1-nsec steps; therefore, a velocity

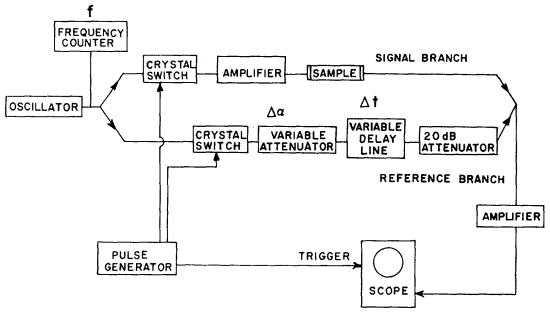

FIG. 1. Block diagram of ultrasonic-phase-comparison measurement technique.

change of (1 nsec)/(5 μsec) = 2×10^{-4} was routinely measured. When more accuracy was desired the rf frequency was changed within a range which corresponded to 1 nsec; the change of the frequency is proportional to the change of the velocity, provided that the transit time of a pulse in the reference branch is negligible relative to that in the signal branch and that the frequency-dependent phase shift introduced by the acoustic transducers and other elements can be neglected (both conditions are satisfied). The frequency was read to one part in 10^6 but the resolution of the method (due to signal-to-noise ratio, etc.) limited the accuracy to ±0.1 nsec. The resolution of the attenuation measurements was ±0.1 dB at 12 MHz. The delay line has a delay-time-dependent insertion loss which is 3.5 dB maximum at the full delay of 1.11 μsec. Therefore only a range corresponding to one wavelength was used, to minimize the change of the insertion loss. This had only a negligible effect at higher frequencies, where the delay-time range was small and the absolute attenuation was high. At lower frequencies corrections were made when necessary. The resolution at 2 MHz was observed to be ±2 nsec and ±0.3 dB.

The absolute values of the velocity and the attenuation were obtained by varying the path length. The sonic cell is described in Sec. III B. The accuracy was checked by using ethanol and water. Agreement to better than 0.3% with the literature values[14] was achieved without difficulty.

B. Sonic cells

Two sonic cells were designed and fabricated, a fixed-path cell and a variable-path cell.

1. Fixed-path cell

A design used by Abraham *et al.* for measurements of liquid-helium properties[15] was adopted for this cell, which is shown in Fig. 2. The main part is composed of a hollow copper block with two end caps, two cartridge heaters, and a thermocouple. A set of coaxial washers and quartz transducers are spring loaded against a gold-plated brass spacer (which is simply a cylinder with both ends flat and parallel). Spacers of various lengths ranging from 0.4 to 2.5 cm were used depending on the frequency. The flat faces of the transducers and ends of the spacer provided a good seal; once the sample was introduced into the spacer it did not leak into the remaining space in the copper block during the course of an experiment.

The cell is placed in a vacuum chamber and suspended by a thin-wall stainless-steel tube to minimize the heat conduction. A power as low as 1 W was enough to maintain the cell at 90°C. Assuming that this heat leak is due solely to the conduction through the tube and that the heat is supplied at the bottom of the cell, the temperature gradient is estimated to be 0.1° from top to bottom. The actual temperature gradient in the sample must be negligibly small.

2. Variable-path cell

To measure absolute values of the velocity and attenuation it is necessary to vary the path length by a known amount, counting the number of wavelengths and measuring the change of the attenuation. The distance swept was measured by a micrometer-screw and dial arrangement. The screw had 40 threads per in. and the dial could easily be read to 1/200 turn; this would provide a resolution of 5×10^{-4} for a length change of 6 mm. Nonreproducibility in the drive mechanism, however, limited the accuracy of the measurements to somewhat less than this ideal value. For one trial measurement, as was mentioned in Sec. III A, an accuracy of 0.3% was achieved and this could be improved slightly by repeated measurements. Because the space between the magnet pole pieces is limited, the screw mechanism must be located far away from the measuring path. The smooth displacement and the maintenance of the parallelism of the transducer faces are assured by using a carefully machined *V*-block and a rider. No effect of a magnetic field on the mechanical parts was noted up to 12.4 kG. The cell is shown in Fig. 3.

Because of the heavy wall connecting the top

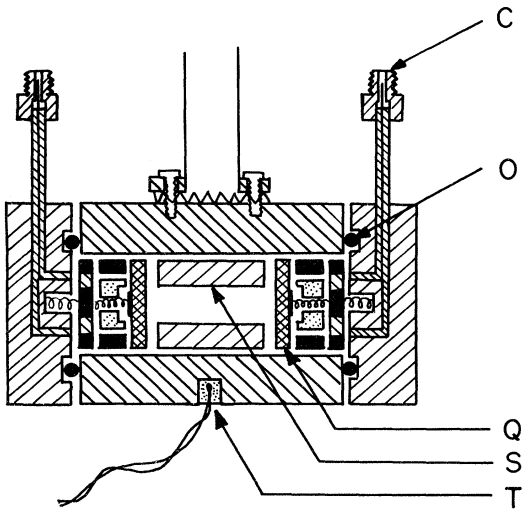

FIG. 2. Fixed-path sonic cell. The following elements are indicated: subminax connector (C), Teflon *O*-ring (O), quartz transducer (Q), brass spacer (S), and thermocouple (T).

plate and lower part the heat leak was relatively high; it took about 3 W to maintain the temperature at 90°C. There is also the heat conduction through the arms that support the transducers. The estimated value of the heat leak through the arms is at most 0.3 W. When the thermal conductivity of the sample is really low, this could cause trouble.

The inside of the cell was evacuated to keep the sample away from oxygen and moisture. This was also effective in getting rid of trapped solvent. A sample kept in this manner did not show any sign of degradation after repeated cycles of heating and cooling.

A unique feature of the cell, which was not anticipated at the time of fabrication, is worth mentioning. Although it takes a rather large amount of sample to fill the cell (about 10 cm^3 compared to 1 cm^3 for the fixed-path cell), the deep trough produces purer material than that loaded. When the liquid-crystal phase separates from the isotropic phase it starts from the bottom because of the higher density. Just below the transition point there are two phases: an impure phase (which is still isotropic because of the lower transition temperature) floating on top of the purer liquid-crystalline phase. When the transducers are immersed deep into the sample the sound passes only through the purer part, thus improving the data significantly. This point will be discussed further in Sec. IV C.

The variable-path cell was constructed after much of the data reported here were already gathered. Thus accurate absolute velocities and attenuations were determined only in the measurements described in Sec. IV C.

C. Temperature control

A copper-constantan thermocouple was used to detect the temperature; the thermal emf was measured against a pre-set potentiometer. The voltage difference was then amplified by a null detector and its output was applied to a KEPCO-regulated power supply, the gain of which was increased by slightly modifying the circuit. The output of the KEPCO was then supplied to the heater. With a careful adjustment of the gain and the maximum heater current a temperature stability of ±0.01°C was achieved.

D. Sample alignment

The sample was aligned by a magnetic field of 12.4 kG. The molecules usually have a positive magnetic anisotropy; thus the director tends to be parallel to the field. The motion of the molecules is a diffusive one with the system seeking an orientational-energy minimum. Therefore a high diffusion probability is important for sample alignment. In a nematic phase the director follows the applied field direction (above a few kG) almost instantaneously (seconds). In a cholesteric material, because of its high viscosity and small magnetic anisotropy, the time constant for readjustment after a change in field direction is fairly long (10–30 min) and the alignment is not complete. It is not easy to rotate the director in the smectic materials once the phase is established (except in the smectic-*C*). In fact, with an applied field of 12.4 kG no sign of rotation of the director in the smectic phase was observed. Therefore aligned smectic phases were all obtained by cooling the sample through the nematic–smectic or isotropic–smectic phase transition in a field.

IV. RESULTS AND DISCUSSIONS

A. Diethyl *p,p'*-azoxybenzoate (DEAB)

Molecular formula.

$C_2H_5OOC\langle O\rangle N{=}NO\langle O\rangle COOC_2H_5$.

Transition temperatures.

Crystal $\overset{114.1\,^\circ C}{\longleftrightarrow}$ Smectic-*A* $\overset{122.6\,^\circ C}{\longleftrightarrow}$ Isotropic.

The velocity anisotropy of this material has been reported elsewhere.[9] There we found a low-fre-

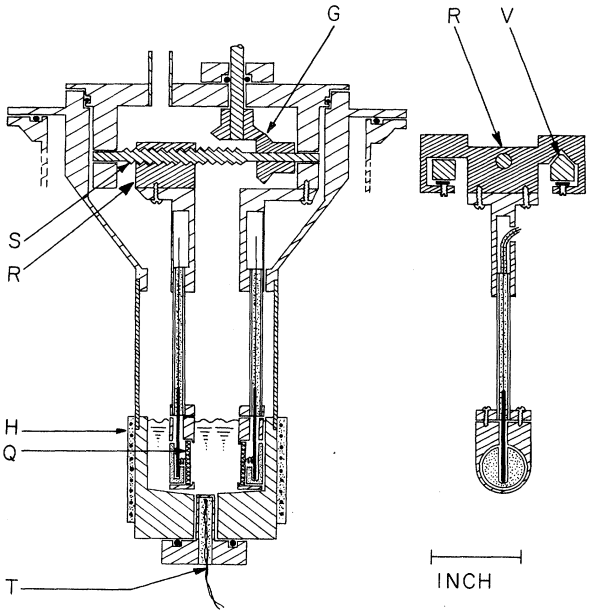

FIG. 3. Variable-path sonic cell. The following elements are indicated: miter and bevel gears (G), rider (R), *V*-block (V), micrometer screw (S), heater (H), quartz transducer (Q), and thermocouple (T).

quency sound-velocity anisotropy of 5%. The values for the C parameters obtained imply that there is a propagating shear wave. In fact, the first motivation of the experiment was to see the direct evidence of the shear-wave propagation in a fluid. An experiment with shear-wave transducers was performed. Only diffuse patterns were obtained, which might well be because of a longitudinal component (since it is difficult to prepare a transducer which provides shear waves exclusively). No clear-cut evidence was observed.

Of course, one can estimate the attenuation of the transverse wave from the data on the longitudinal wave. As an example the data at 12 MHz at 115.3°C are shown in Fig. 4. The absolute value was obtained by measuring the height of successive echoes. Because of the existence of spurious amplitude-degrading processes (e.g., transducer alignment) it is only approximately correct, but this will suffice for the following discussion. The curve is the best fit using Eq. (7), which yields $D_{11}=3.47$, $D_{33}=7.12$, and $2D_{13}+4D_{44}-D_{11}-D_{33}=-2.97$ (P cm^3/g). A simple calculation shows that the attenuation of the shear wave may be written as

$$\alpha=(\omega^2/2V^3)[D_{44}+(D_{11}+D_{33}-2D_{13}-4D_{44})\times\sin^2\theta\cos^2\theta], \tag{14}$$

where V is the shear-wave velocity, the maximum of which, calculated with known C's, occurs at $\theta=45°$ and is $V=0.24\times10^5$ cm/sec. Because D_{13} and D_{44} cannot be determined independently we try the most favorable case allowed by the dynamic stability. If the dominant attenuation mechanism is the viscosity (which is likely to be the case) the dynamic stability conditions for the viscosity result in D_{11}, D_{33}, $D_{44}>0$, and $D_{11}D_{33}-D_{13}^2>0$. Because the value for the combination $D_{11}+D_{33}-2D_{13}-4D_{44}$ is fixed, the minimum α in Eq. (14) is realized when D_{44} is smallest; hence D_{13} is largest. D_{13}^2 cannot exceed $D_{11}D_{33}$; therefore D_{13} is at most 4.97, which results in $D_{44}=1.40$ (P cm^3/g). When these values are inserted in Eq. (14) a shear-wave attenuation divided by the frequency squared of 26.6×10^{-12} dB sec^2/cm results; this is two orders of magnitude larger than the attenuation of the longitudinal wave. There is almost no chance of seeing the signal, if any, using a standard pulse-echo arrangement.

B. *p*-Cyanobenzylidene-*p*-*n*-octyloxyaniline (CBOOA)

Molecular formula.

$N\equiv C\langle O\rangle CH=N\langle O\rangle OC_8H_{17}$.

Transition temperatures.

Crystal $\overset{73.2^\circ C}{\longleftrightarrow}$ Smectic-A $\overset{82.9^\circ C}{\longleftrightarrow}$ Nematic $\overset{107.5^\circ C}{\longleftrightarrow}$ Isotropic.

This material was chosen for two reasons: (i) the nematic-smectic-A (N-A) transition was suggested to be second order and the matter was controversial; (ii) continuous measurement across the N-A transition point enables us to study the quantitative differences between the smectic and the nematic phases.

The material was recrystallized from heptane solution. This easily yielded single crystals ~1 mm wide by 10 mm long. The material was kept at about 106°C (close to the isotropic–nematic transition point) for 2 h *in vacuo*. After 20–40 h of measurement no change of the N-A transition temperature (T_c) of 82.9 ± 0.2°C was found. T_c was determined optically by a sudden change of the material to a less turbid state.

It was first suggested by McMillan[16] that the N-A transition might be second order, because a specific-heat anomaly had not been observed. Many experiments[17] close to T_c showed strong pretransitional effects which were subsequently analyzed in the context of a second-order phase transition. A small but finite specific-volume change was recently found,[18] however, and hence the transition is first order. A "bump" in the specific heat was also found[19] in a purified sample.

The occurrence of a pronounced maximum in the attenuation and a minimum in the velocity at a first-order transition (as in isotropic–nematic transitions) is well known. We measured the

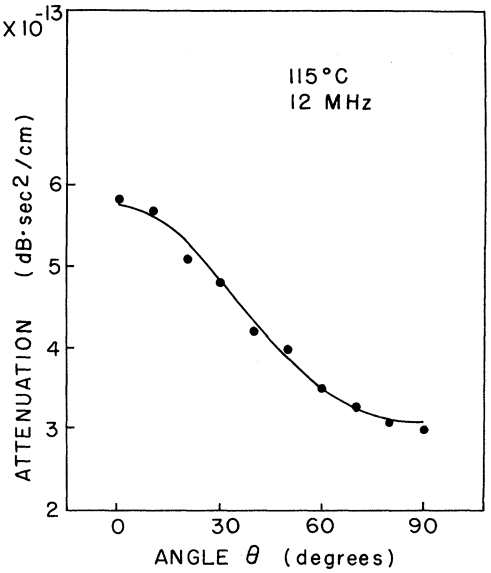

FIG. 4. Attenuation anisotropy in DEAB. The curve is a least-squares fit.

velocity and attenuation change with an applied field. The frequency ranged from 2 to 36 MHz. The data are shown in Figs. 5 and 6. Other data at 4, 10, 20, and 36 MHz were practically the same. As is seen in Fig. 5, no drastic change occurs at the transition point except that the slope of the velocity as a function of the temperature changes slightly. At isotropic–nematic transitions strong dispersion is commonly observed, which tends to obscure the transition. Therefore the chance of seeing transitional effects is highest when the frequency is lowest. For this reason the data at 2 MHz were taken in 0.1-deg intervals; although these data, shown in Fig. 6, do not reveal any drastic change either, we note a slight flattening of the slope of the velocity around 83.3°C and a small "hump" in the parallel field attenuation around 83.7°C. Because the above-stated changes are the same order of magnitude as the scatter of the data we can only say that the transitional effects, if any, are very small, in spite of the large pretransitional behavior in other experiments.

It is possible that our sample was not pure enough. Because the specific-volume change was observed[18] even in dirty samples, it is unlikely that the impurity content was the reason. It could be that the lowest frequency, 2 MHz, is not low enough compared to the relaxation time of the fluctuations (temporary appearance of the smectic order in the nematic phase). A phase diagram[20] of CBOOA shows that the coexistence curve of the smectic-A and nematic phases is almost vertical, i.e., $dT/dp \sim 0$. This means that the pressure field (sound) does not couple with the transitional behavior and this agrees with our observation.

As was stated before, we can make a quantitative macroscopic comparison between the nematic

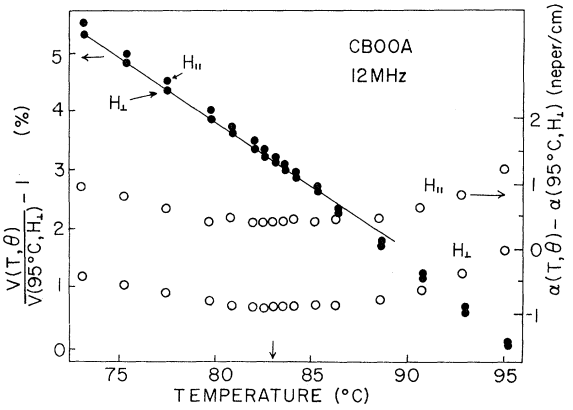

FIG. 5. Temperature variation of the velocity and attenuation with a field parallel ($H_\parallel$) and perpendicular ($H_\perp$) to the sound propagation direction in CBOOA.

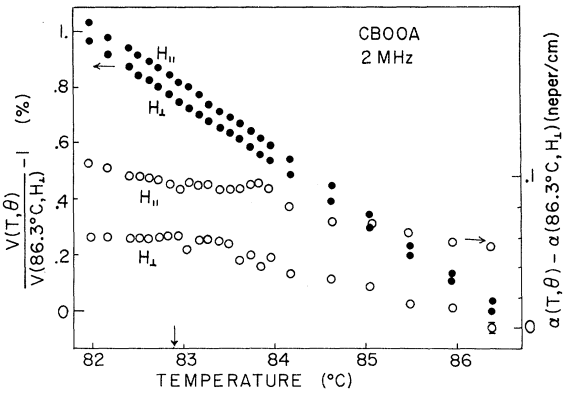

FIG. 6. Same as for Fig. 5, at 2 MHz.

and smectic-A phases in this material since the intermolecular forces should be the same in both phases. Typical anisotropy data in the nematic phase are shown in Fig. 7, where the isotropic part is subtracted. The theoretical prediction in Sec. II C is that there should not be any velocity anisotropy in the nematic phase. The data, however, clearly show anisotropy. The curves are the best fit using Eqs. (6) and (7).

Now let us consider the physical idea behind the theory which brings about the velocity anisotropy in a smectic-A but not in a nematic material. There are two different compressibilities in the smectic-A. This means that when the planes are compressed, say, then the stress parallel to the normal is different from that perpendicular to it. This difference should be supported by the very molecular forces that make a planar arrangement of the molecules more stable than a nematic arrangement. In a nematic phase, on the other hand, because there is no restriction on the distribution of the centers of mass of the molecules, any uniaxial compression, either parallel or perpendicular to the director, results in the same distribu-

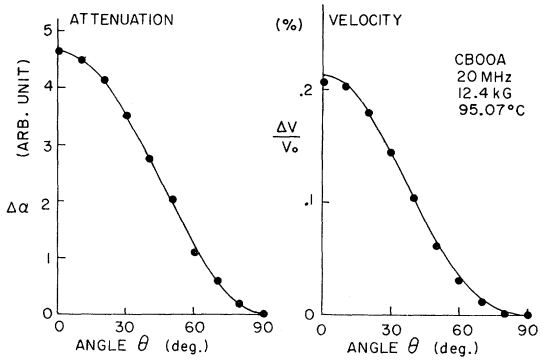

FIG. 7. Velocity and attenuation anisotropy in CBOOA in the nematic phase.

tion of molecules; i.e., the distribution is determined only by the pressure and not by the direction in which it is applied. The molecules simply flow driven by the stress gradient, if it exists, and after the rearrangement no stress gradient remains. Any shear caused by the director deformation is of higher order in $\vec{q}$. Thus a nematic material has an isotropic compressibility and there should not be a velocity anisotropy. We have to remember, however, that the molecular rearrangement process is a diffusive one. It takes time for molecules to establish a new equilibrium. Therefore for short times (i.e., for high frequencies) the uniaxial compressibility can be anisotropic.

The data similar to those shown in Fig. 7 at various frequencies were analyzed to obtain the C's and D's. Following the discussion in Sec. II B, we first examined the quantities $C_{33}-C_{11}$ and $D_{33}-D_{11}$, which are shown in Fig. 8. The solid lines are a least-squares fit of the data (filled circles) to Eq. (9). The agreement is reasonable and we can determine three parameters τ, Δ, and $C_{33}(0)-C_{11}(0)$. At 77.54°C the material is in the smectic-A phase and at 90.74°C in the nematic phase. In accordance with our expectation, while $C_{33}(0)-C_{11}(0)$ [which is equivalent to $V^2(0°)-V^2(90°)$] is nonzero in the smectic-A phase, it actually extrapolates to zero in the nematic phase

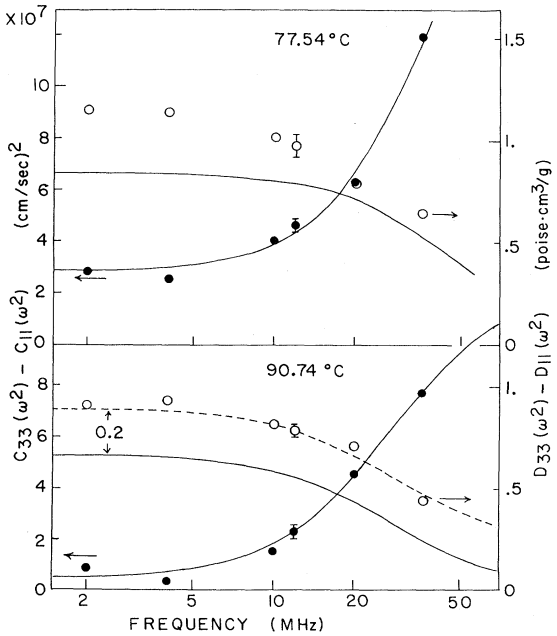

FIG. 8. Dispersion in the anisotropic part of the parameters, $C_{33}-C_{11}$ and $D_{33}-D_{11}$, in CBOOA. It is in the nematic phase at 90.74 °C and in the smectic-A phase at 77.54 °C.

within our experimental error. We note that there is a strong dispersion in the smectic-A phase also. In view of this fact some caution must be taken in interpreting light-scattering data, since this technique probes the behavior of very-high-frequency sound waves.

With τ and Δ determined, $D_{33}(\omega^2)-D_{11}(\omega^2)$ can be calculated uniquely using Eq. (10); this quantity is also shown by solid lines in Fig. 8. The data (open circles) are always above these lines. This can be explained easily. In the derivation of the dissipative part [Eq. (10)] it is assumed that the dissipation is due solely to the existence of a relaxational process. But we also have so-called classical dissipation due to viscosities even when there is no relaxational process. In fact, in terms of viscosity coefficients, $\rho(D_{33}-D_{11})=\eta_1-\eta_2-\eta_4$. If we assume that the bulk-viscosity part of $\eta_1-\eta_2-\eta_4$ is accounted for by Eq. (10) and that the shear-viscosity part has a frequency-independent contribution to the attenuation, a value of 0.2 P ($\rho\sim1$ g/cm^3) at 90.7°C for the shear part results in the dotted line in Fig. 8. Note that in the typical nematics p-azoxyanizole and p-azoxyphenetole this quantity, $\eta_1-\eta_2-\eta_4$, is 0.334 and 0.140 P,[21] respectively. In both materials no strong dispersion was seen between 3 and 18 MHz; thus it is reasonable to assign it to the shear viscosity. In the smectic-A phase the addition of a simple frequency-independent constant is not sufficient to explain the difference.

The combinations $C_{11}+C_{33}-2C_{13}$ and $D_{11}+D_{33}-2D_{13}-4D_{44}$ have expressions similar to Eqs. (9) and (10). The data are shown in Fig. 9. Because of the large uncertainties of the points we did not attempt to fit any curve to them. Note that, although the absolute values of the velocity and attenuation do not change across the transition point, these combinations do. The quantity $C_{11}+C_{33}-2C_{13}$ is associated with the deformation of the

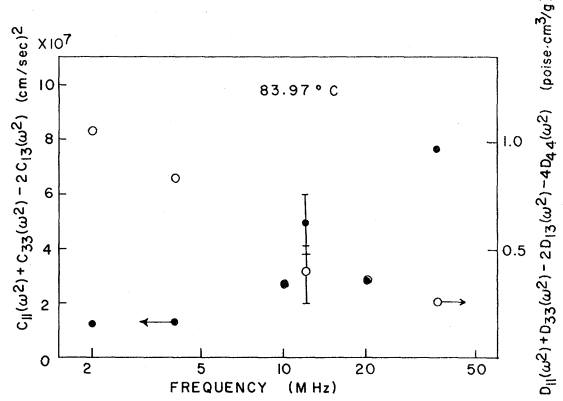

FIG. 9. Dispersion in the shear part of the parameters $C_{11}+C_{33}-2C_{13}$ and $D_{11}+D_{33}-2D_{13}-4D_{44}$, in CBOOA.

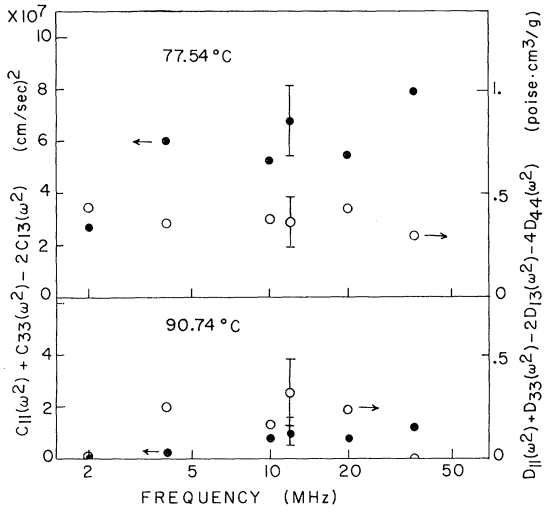

FIG. 10. Same as for Fig. 9, but close to the nematic–smectic-A transition.

smectic planes, $(\partial \phi_3/\partial \nabla_3 x)_{s\rho}$. As is seen in Fig. 9, this quantity is almost zero in the nematic phase and is nonzero in the smectic phase, as expected. A weak frequency dependence is discernible. The corresponding dissipative part also shows smaller values in the nematic state than in the smectic state, but the difference is less pronounced because the existence of the shear viscosity is not directly related to the presence of the smectic order. The combinations of parameters are strongly frequency dependent around T_c (Fig. 10), indicating a slow process (time constant is 10^{-7} sec or slower). This may be due to a coupling between the director (fast mode) and density change manifested by the temporal appearance of the smectic order.

The hydrodynamic behavior of $C_{33} - C_{11}$, which is an indicator of the smectic order, and the relaxation time constant τ as functions of temperature are shown in Fig. 11. A sudden increase of $C_{33}(0) - C_{11}(0)$ from zero around T_c is clearly seen. In fact, the increase happens at a higher temperature than T_c, probably because a less turbid state, which was used to determine T_c optically, is realized only after all transitional fluctuations have ceased. Many experiments[17] on the pretransitional divergence of the Frank elastic constants essentially measure the squared average of the smectic order parameter $\langle \psi^2 \rangle$. Because our measurement is on a static property ($\omega \to 0$) and the velocity anisotropy is a measure of the strength

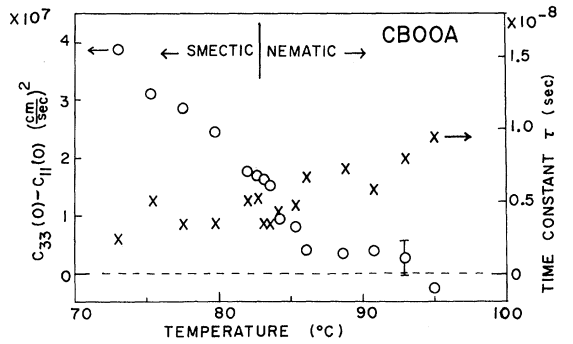

FIG. 11. Temperature dependence of the zero-frequency anisotropy, $C_{33}(0) - C_{11}(0)$, and the relaxation time constant τ.

of the planar arrangement, the quantity $C_{33}(0) - C_{11}(0)$ should go to zero smoothly as $\langle \psi \rangle$ goes to zero. The abrupt increase of $C_{33}(0) - C_{11}(0)$ then suggests that the order parameter does not start from zero at the transition point and hence the transition is first order.

Surprisingly, there is no apparent change in τ across T_c besides a monotonic decrease. Because the diffusion of molecules between planes in the smectic phase must be much less probable than the equivalent diffusion in the nematic phase, the continuity of τ seems to indicate that the relaxational process involves the end chains of the molecules.

One characteristic of CBOOA is the smallness of the anisotropy $(C_{33} - C_{11})/C_{11}$. For instance, DEAB has a value about 7.5% and other materials show larger anisotropies,[22] whereas in CBOOA it is less than 0.3%. Nevertheless, the smectic structure appears fairly rigid, since no change in the velocity occurred on rotating the magnetic field at 77°C and waiting for a period of an hour.

The absolute value of the velocity and attenuation at 95°C and 2 MHz with the field perpendicular to the propagation direction was found to be $1.21 \pm 0.07 \times 10^5$ cm/sec and 0.24 ± 0.01 Np/cm, respectively.

C. Ethyl-*p*-[(*p*-methoxybenzylidene) amino] cinnamate (EMBAC)

Molecular formula.

CH_3O ⟨O⟩ $CH=N$ ⟨O⟩ $CH=CHCOOC_2H_5$.

Transition temperatures.

Crystal II → Crystal I $\overset{107\,^\circ C}{\longleftrightarrow}$ Smectic-A $\overset{117.6\,^\circ C}{\longleftrightarrow}$ Nematic $\overset{138.5\,^\circ C}{\longleftrightarrow}$ Isotropic

80 °C Smectic-B 91 °C.

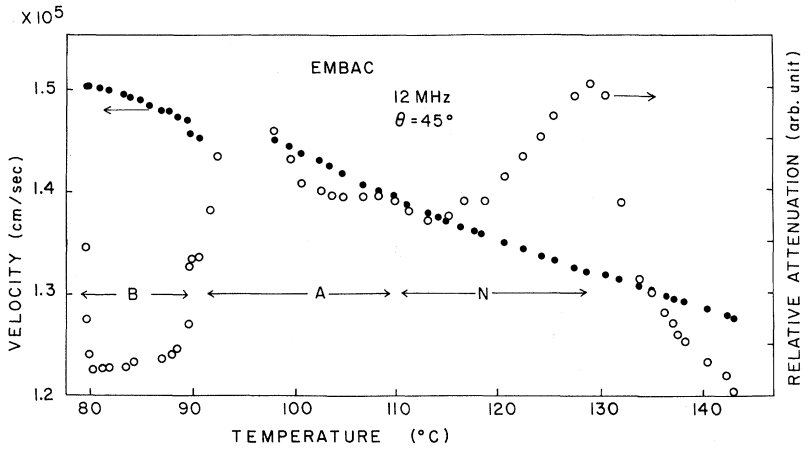

FIG. 12. Temperature variation of the velocity and attenuation in the nonpurified EMBAC with a field at 45° relative to the sound propagation direction. Here N, A, and B, respectively, denote the nematic, smectic-A, and smectic-B phases.

(This diagram is according to Demus and Sackman.[23] Because the transition temperatures are very sensitive to the impurity level the above diagram is given only for the purpose of reference.)

So far we have seen that the theory for the smectic-A and nematic materials works fairly well. It is of interest to extend the experiments to a smectic-B phase. EMBAC was chosen for this purpose. The variable-path cell was employed as well as the fixed-path cell. It was the use of both cells that revealed the strong dependence of the transition temperatures on impurities and the strong dispersion.

Both purified and nonpurified samples were used. The purification was done by recrystallization from either heptane or ethanol solution. The purified sample was introduced into the variable-path cell, which was kept at pressures lower than 0.1 Torr. The sample obtained and maintained in this manner showed no sign of degradation, which is easily detected by a decrease of the transition temperatures, after repeated heating and cooling cycles for two months. The nonpurified samples, on the other hand, did not produce consistent data once they were solidified and remelted again. The purified sample was also used for the fixed-path cell and the quality of data was poorer than those of the nonpurified sample. The sample was inspected afterwards and segregation was found; the top part of the sample had a 10°-lower N-A transition temperature than the bottom portion. A careful examination showed a distinct difference and a clear boundary between the top quarter and the remainder of the sample. The top layer could be a eutectic mixture of EMBAC and the solvent, which was not easily removed by placing the material *in vacuo* at an elevated temperature. In the fixed-path cell the sample is confined in the spacer, and the sound passes through the whole sample. Therefore if the material is of a quality as poor as the above one, the measured quantity is some kind of an average of pure and impure material. On the other hand, in the variable-path cell, as was discussed in Sec. II C 1, segregation does not affect the experiment.

A quick (0.3 deg/min) temperature sweep with the field at 45° over the whole mesomorphic range is shown in Fig. 12; the sample was not purified. The high attenuation at the smectic-A–smectic-B (A-B) transition is in strong contrast to the smooth N-A transition. Temperature sweeps over the isotropic–nematic–smectic-A region of both purified and nonpurified samples without an external field are shown in Figs. 13–15. The transitions are very well seen in the purified sample. Note further that the transition temperatures in the nonpurified sample are consistently lowered by about 9 deg. A typical transitional behavior, the velocity minimum and attenuation maximum, is obvious at the isotropic–nematic

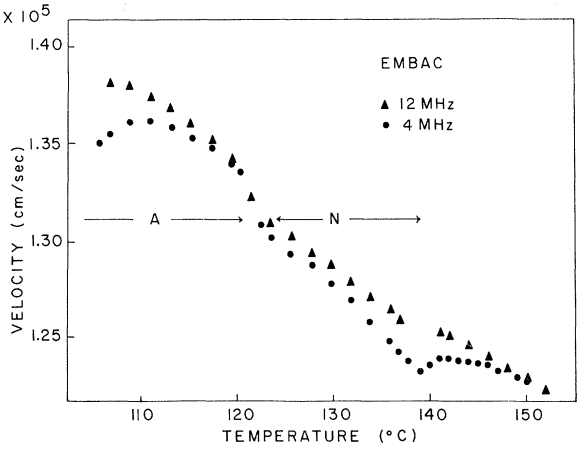

FIG. 13. Temperature variation of the sound velocity in the purified EMBAC with a field. Note the decrease at the isotropic to nematic transition and at the smectic-A–smectic-B transition.

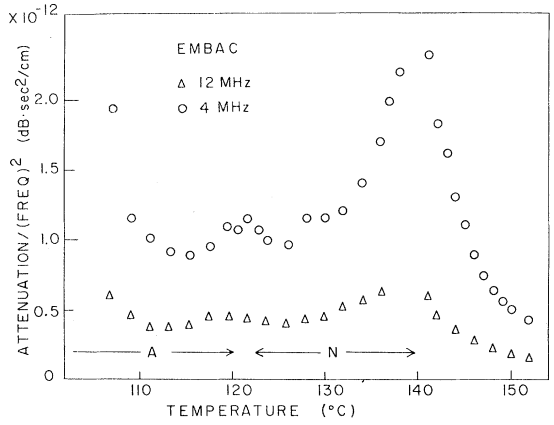

FIG. 14. Temperature variation of the sound attenuation coefficient divided by the frequency squared in the purified EMBAC without a field. Note the peak at each phase transition.

(I-N) transition. Although no velocity dip is found at the N-A transition, a small hump in the attenuation is seen. This was not found in the N-A transition in CBOOA. The dispersion is also very large throughout the temperature range. More interesting is the "softening" of the system toward the A-B transition. The change is even more drastic, as is shown in Fig. 16, when a magnetic field is applied. The velocity anisotropy increases at the N-A transition as expected. However, the velocities with the field at 0° and 30° relative to the sound propagation direction increase monotonically, whereas those with the field at 60° and 90° bend down. This striking difference clearly illustrates that the phase transition occurs within the planes but not between the planes. The almost linear increase of the velocity with the field at 0° indicates that there is no rearrangement between planes, which might occur if the transition is to a plastic crystal phase rather than a smectic-*B* phase. The above observation fits nicely with our understanding of the A-B transition: It is a two-dimensional liquid-to-solid transition. It seems that this A-B transition offers great potential for an interplay of theory and experiment. A simple calculation of the dynamics of hard circular disks, for instance, may be relevant to the experiments. A two-dimensional specific-volume-change measurement may be feasible without much elaboration.

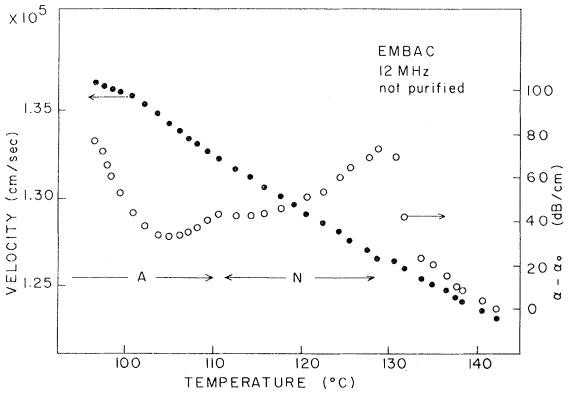

FIG. 15. Temperature dependence of the velocity and attenuation in nonpurified EMBAC without a field.

The anisotropy in the smectic-*A* phase is strange, as is seen in Fig. 16; the velocity with the field at 30° is higher than that at 0° and the velocity at 60° is lower than that at 90°; i.e., both the maximum and the minimum of the velocity occur off the symmetry axes. This is better viewed in Fig. 17, where the field was rotated while the temperature was fixed. The sample was not purified. In the smectic phase rotation of the field should not affect the orientation, but it has been observed[24,25] that impurities "lubricate" the system so that the field can actually rotate major parts of the sample. In a purified sample the rotation of the field produced only a small sluggish change of the velocity. Thus Fig. 17 may not show the full anisotropy but it still uncovers qualitative features; the velocity has a maximum around 85 °C and a minimum at 55 °C. A three-parameter fit cannot reproduce this type of anisotropy. We do not attempt further analysis until more evidence is accumulated.

The anisotropy of the smectic-*B* phase, which is the main theme of this section, is seen in Figs.

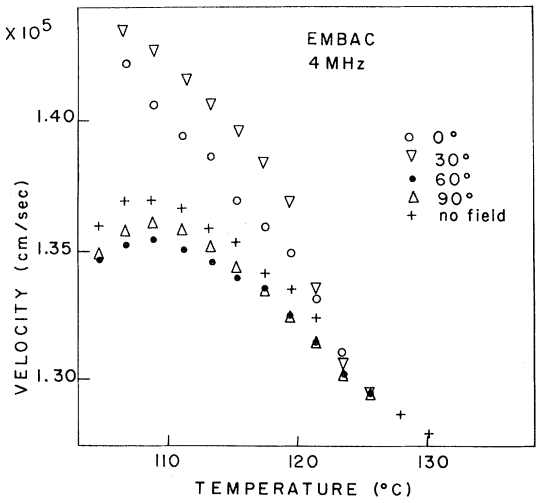

FIG. 16. Temperature dependence of the velocity with the field at various angles in the purified EMBAC in the nematic and smectic-*A* phase. Note the pretransitional reduction in the velocity with the field at 60° and 90°.

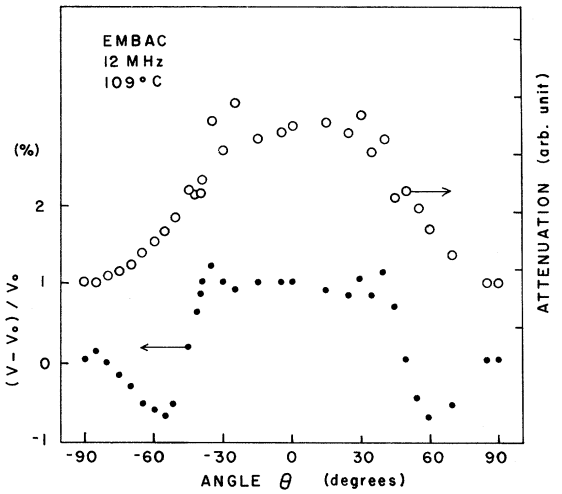

FIG. 17. Velocity and attenuation anisotropy in nonpurified EMBAC in the smectic-A phase. The field was rotated while the temperature was kept constant.

18 and 19. Because of the large attenuation at the A-B transition the signal could not be continuously traced from the smectic-A phase. The data in the smectic-B phase therefore have an ambiguity of a multiple of the sound wavelength. Hence we used the time-of-flight method as well as the interference method. Because of the poor accuracy of the time-of-flight measurement we could not determine the absolute values of the velocity for each frequency separately. Therefore the absolute value at $\theta = 90°$ was fixed for all frequencies at each temperature and the velocity anisotropy relative to it was plotted in Fig. 18. The data were all taken in nonpurified samples. It was difficult to keep a purified sample in the smectic-B phase; the sample tends to go into the solid phase not long after the smectic-B phase is reached. It may be that impurities stabilize the B phase. The boundary plays a role to some extent because even in a purified sample it was relatively easy to obtain a stable smectic-B phase when the layers were parallel to the transducers (the 0° position). At 83.2 °C the absolute value of the attenuation divided by the frequency squared in the above case was 0.370 and 2.03×10^{-12} dB sec^2/cm at 12 and 4 MHz, respectively.

The data were analyzed using three parameters (C_{11}, C_{13}, and C_{33}) for the reactive part and four (D_{11}, D_{13}, D_{33}, and D_{44}) for the dissipative part. The attenuation was found to be less reproducible but the velocity anisotropies at 12, 5, and 2 MHZ were in fair agreement with each other.

The velocity anisotropy shows that the B phase has a larger anisotropy but no qualitative difference from that of a typical smectic-A phase. A fourth parameter, C_{44}, was also tried. The result was that C_{44} is small but negative, $C_{44}/C_{11} = -5\times10^{-2}$. Of course, a negative C_{44} is nonphysical. We subsequently tried various fixed C_{44} values to see the significance. One example is shown in Fig. 20. Two values $C_{44} = -0.126\times10^{10}$ (cm/sec)^2 (by least squares) and $C_{44} = 0$ give almost identical curves, but as soon as C_{44} becomes positive [$C_{44} = 0.01$ and 0.1×10^{10} (cm/sec)^2], the deviation is noticeable. From this observation and the physical consideration we choose to fix $C_{44} = 0$. The solid curves in Fig. 18 are the best fit obtained in this way. The value of C_{44} is a key to distin-

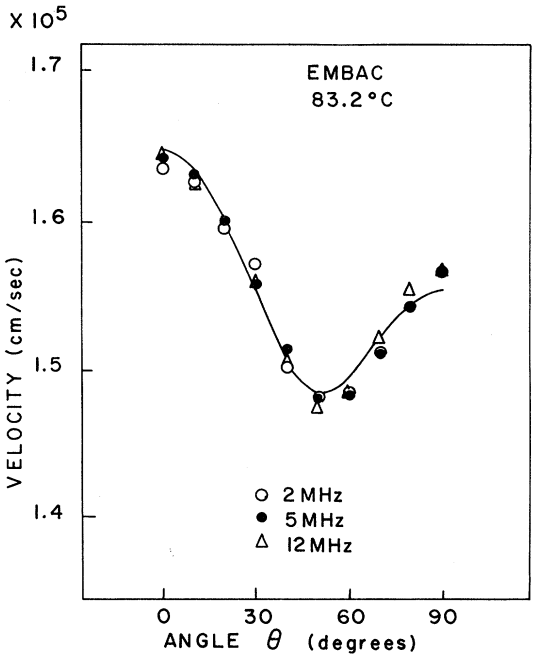

FIG. 18. Velocity anisotropy in nonpurified EMBAC in the smectic-B phase.

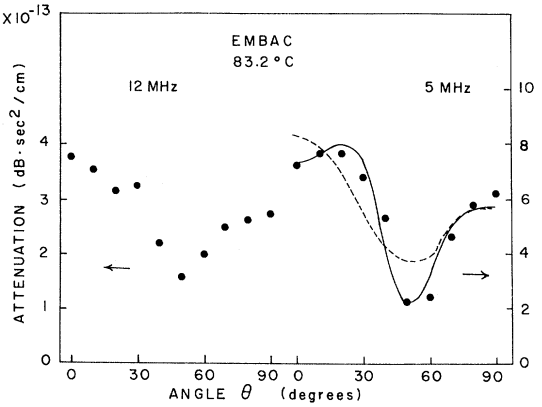

FIG. 19. Attenuation anisotropy in nonpurified EMBAC in the smectic-B phase.

guishing a smectic-B phase from a plastic crystal, and the matter should be settled by more sensitive methods (e.g., shear-wave propagation along the plane normal). We attempted shear-wave measurements, but in vain so far.

The attenuation anisotropy (Fig. 19) is puzzling. There was a qualitative difference between the anisotropy at 12 MHz and that at 5 MHz. The data at 12 MHz did not reproduce well. The analysis was done only for the data at 5 MHz. Because the assumption of small velocity anisotropy used to derive Eq. (7) may not be justified in this case, we directly calculated the imaginary part of Eq. (4) with the C's obtained above. All four D's are then independent. The solid curves in Fig. 19 were obtained by the least-squares technique. The parameters at 83.2 °C are $D_{11}=12.3$, $D_{13}=-1042$, $D_{33}=19.2$, and $D_{44}=517$ (P cm^3/g). Those parameters, however, seriously violate the dynamical stability conditions. A fit using Eq. (7) is shown in Fig. 19 by broken curves. The parameters are now $D_{11}=12.3$, $D_{33}=21.5$, and $2D_{13}+4D_{44}-D_{11}-D_{33}=-37.8$ (P cm^3/g). (The last value for the four-parameter fit is −47.5.) One can choose certain values for D_{13} at will to meet the stability conditions, but the fit is worsened considerably.

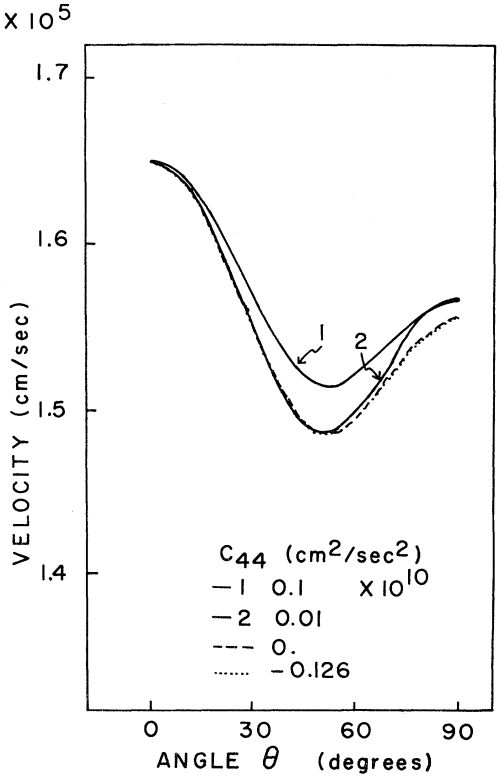

FIG. 20. Significance of the uniform shear constant C_{44} in the velocity-anisotropy fit.

As is discussed in Appendix A, the formalism outlined in Sec. II B is, strictly speaking, only valid when the thermal expansion and the vacancy diffusion are neglected. In the presence of these effects a term like $D'\sin^2\theta\cos^4\theta$ also appears. The stability criteria for the phenomenological D coefficients does not hold then because each parameter has several contributions. Because neither the heat capacity nor the thermal conductivity is known, we cannot calculate the parameter D'. A rough estimation can be done, however, as follows. In the nematics, representative values of the thermal conductivity,[26] κ, and the heat capacity at constant pressure,[27] C_p, are $\kappa=3\times10^{-4}$ cal/cm sec °C and $C_p=1000$ J/°C mol, respectively. If we assume that $(C_p-C_v)/C_p\sim3\times10^{-2}$, then we obtain $D'=1.1\times10^{-5}$ P cm^3/g. Because the D's are of the order of 10 P cm^3/g, any thermal effect is normally negligible.

The anomalous attenuation anisotropy remains unexplained. One may relate this anomaly to the fact that this smectic-B phase is a metastable state. The boundary effect could be large. More experiments in a smectic-B phase of other materials are needed.

Finally, we notice that the attenuation in the unoriented sample is higher than the attenuation maximum. This means that the domain boundaries are important in determining the polycrystalline attenuation. Let us recall[28] that the attenuation of sound in a polycrystal can be very high compared to that of a single crystal because of the anomalous buildup of temperature gradients in narrow regions at the grain boundaries. In a nematic or a smectic-A phase such a boundary effect may be negligibly small; as a result of the softness of those structures the boundary may well be blurred.

D. p-p'-Heptyloxyazoxybenzene (HAB)

Molecular formula.

$C_7H_{15}O\langle\bigcirc\rangle NO=N\langle\bigcirc\rangle OC_7H_{15}$.

Transition temperatures.

$$\text{Crystal} \xleftrightarrow{74.4\,^\circ\text{C}} \text{Smectic-}C \xleftrightarrow{95.9\,^\circ\text{C}} \text{Nematic} \xleftrightarrow{124.0\,^\circ\text{C}} \text{Isotropic}.$$

The experiments were done only at 12 MHz and are still in a preliminary stage of investigation.

Azoxy compounds are rather stable relative to other liquid-crystalline materials, so we did not attempt any purification. The temperature variations of the velocity and attenuation with the field parallel and perpendicular to the propagation di-

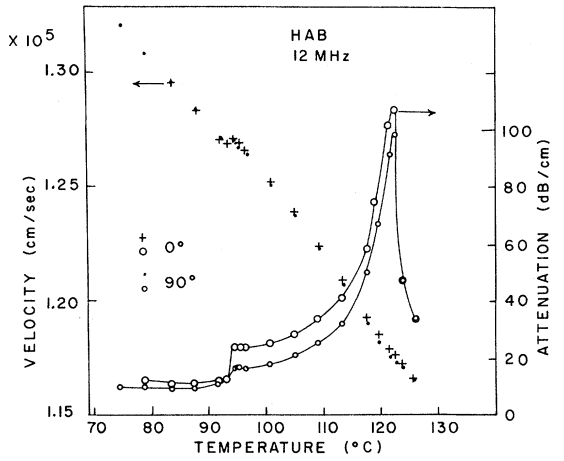

FIG. 21. Temperature variation of the velocity and attenuation in HAB with a field parallel and perpendicular to the sound propagation direction. Note the velocity minimum and the abrupt decrease of attenuation.

rection are shown in Fig. 21. The isotropic–nematic transition has the familiar features. The velocity and attenuation anisotropy in the nematic phase (Fig. 22) reveals nothing new. A striking feature, however, is the smallness of the anisotropy in the smectic-*C* phase. Below 95 °C only a slight difference is seen between the attenuation with the field parallel and perpendicular to the propagation direction. This is in contrast to the cases of smectic-*A* and -*B* materials. Because it is natural to assume that a lower-temperature phase is more solidlike than higher ones, the apparent smallness of anisotropy compared to that of the nematic phase must be explained not by a possible lack of anisotropy in the smectic-*C* phase itself but by a structural complexity.

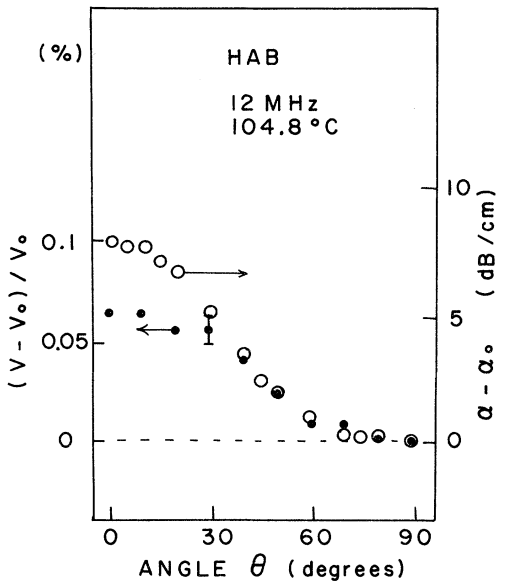

FIG. 22. Velocity and attenuation anisotropy in HAB in the nematic phase.

It has been shown by optical[29] and NMR[24,30] experiments that HAB has a tilt angle close to 45°. When the smectic-*C* phase is obtained by cooling through the nematic to smectic-*C* (N-C) transition point the molecules are parallel to the field. The normal to the smectic planes, however, cannot be specified by a uniaxial external field. Therefore in the smectic-*C* phase thus obtained, grains or domains are expected with the orientation of their plane normal evenly distributed over a cone with an apex angle of 90°, and with their axis parallel to the field (Fig. 23). The field was rotated with such an "oriented" sample; the anisotropy is shown in Fig. 24. It is known from NMR measurements that molecules in the smectic-*C* planes can rotate on a cone of the tilt angle, in contrast to the smectic-*A* and -*B* phases. When the field is rotated molecules reorient themselves, within the range allowed under the condition that the molecules are at 45° from the plane normal, to minimize the orientational energy. There is no anisotropy in the velocity within the resolution and the attenuation anisotropy is a factor of 2 smaller than that in the nematic case. That the movement of the molecules is free is shown in Fig. 24. A field of 2.9 kG produces 80% of the effect observed with a field of 12.4 kG, and at 5.6 kG the effect appears saturated.

Two remarks about the smectic-*C* phase are readily made: (a) The absence of a velocity anisotropy in spite of the evidence of molecular reorientation suggests that the velocity anisotropy

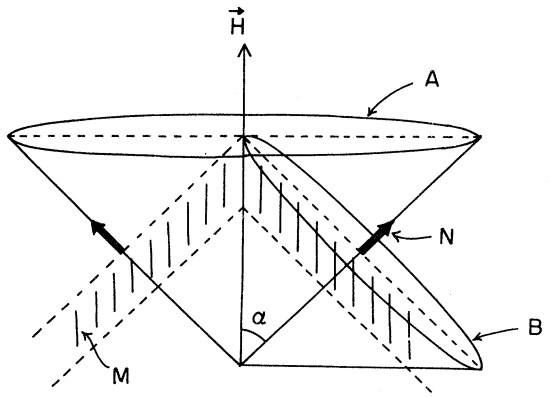

FIG. 23. Molecular arrangement in the smectic-*C* phase in a magnetic field. Here $\vec{H}$ is the magnetic field, N is the plane normal that lies in the plane of the paper, M are the molecules, α is the molecular tilt angle, A is the cone of possible plane normals, B is the cone of possible orientations of molecules that belong to the particular plane normal N.

does not depend on the orientation of the molecules within the plane, but only on the direction of the sound propagation relative to the plane normal; the planes do not move. This is in agreement with the absence of a velocity anisotropy in the nematic phase in the hydrodynamic limit. Even the anisotropy due to dispersion, which exists in the nematic phase, is not found. In fact, in the elasto-hydrodynamic theory[4] the reactive part of the smectic-C phase is treated the same way as that of the smectic-A phase neglecting the molecular tilt. (b) Conversely, the attenuation anisotropy (Fig. 24) indicates that at least part of the attenuation originates from processes where the orientation of each molecule relative to the propagation direction is important; that part of the attenuation which is sensitive to the direction of the plane normal relative to the propagation direction is "frozen in" in this experiment. It is not known how the molecular orientation effects measured in sound propagation enter the transport coefficients (η, κ, ξ, and ζ).

There is a noticeable decrease in attenuation at the N-C transition. This may be understood as a sudden decrease of diffusivity which is caused by the layered structure. A decrease of the velocity is also found at the transition.

Compared with intense studies of the N-A transition, the N-C transition has rarely been studied. The absence of an attenuation maximum coupled with the existence of a distinct velocity minimum is very unusual; the frequency dependence is also interesting. We can separate the effect of the planar structure from that of the molecular orientation by observing the difference in anisotropy when the material is field cooled and when the field is rotated after the smectic-C phase is obtained.

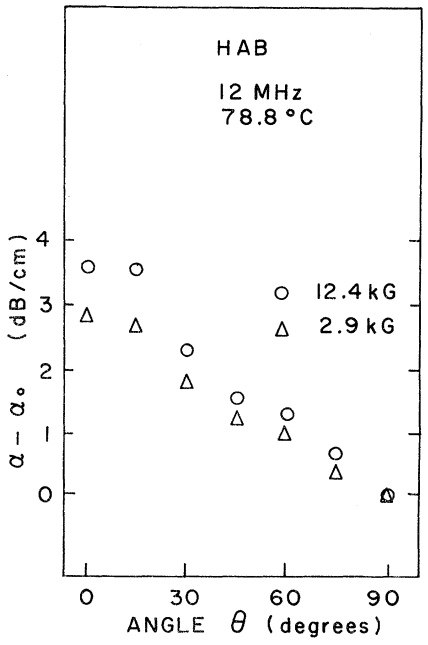

FIG. 24. Magnetic-field-rotation diagram of the sound attenuation in HAB in the smectic-C phase.

E. Cholesteryl chloride and cholesteryl myristate mixture

Molecular formula.

Cholesteryl chloride (CC) $ClC_{27}H_{45}$;

Cholesteryl myristate (CM)

$CH_3(CH_2)_{12}COOC_{27}H_{45}$;

CC:CM = 1.75:1 by weight.

Transition temperature.

Cholesteric to Isotropic at 68 °C.

Most of the cholesteric materials have positive magnetic anisotropy; i.e., molecules tend to be parallel to a field. Hence the helix axis lies perpendicular to the field and it is not possible to obtain a uniform sample. The above mixture, however, has been known[31] to have a negative magnetic anisotropy. Thus the helix axis is parallel to the field, and the sample is presumably uniform.

A temperature sweep with the pitch axis parallel to the sound propagation direction is shown in Fig. 25. The high attenuation prevented us from obtaining a reasonable absolute attenuation measurement (only one echo was observed and the variable-path cell was not available at this time); therefore only its change relative to that at 87.6 °C is shown. The chirality of the helix switches its sign at 42 °C; i.e., at 42 °C the pitch is infinitely long.

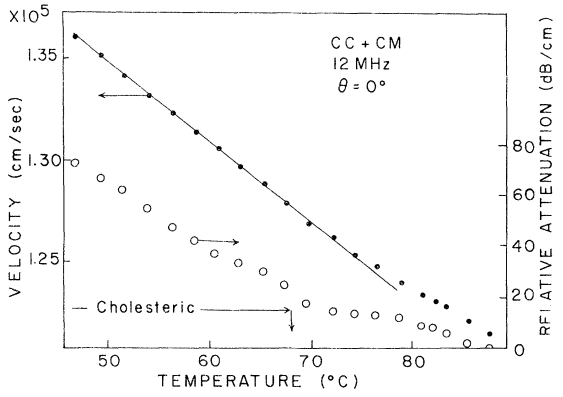

FIG. 25. Temperature dependence of the velocity and attenuation in a cholesteryl chloride and cholesteryl myristate mixture (CC + CM) with a field parallel to the sound propagation direction.

It would be quite interesting if one could observe an interference when the sound wavelength matches the pitch. Unfortunately the attenuation is so high at lower temperatures we could not make measurements around this chirality change point.

To observe the anisotropy we rotated the magnet at a fixed temperature. The cholesteric phase was first reached without a field and the field was applied subsequently. The time dependence of the velocity change in such a process is shown in Fig. 26, where the temperature was held at 51.5 °C and at $t=0$ a magnetic field of 12.4 kG was applied perpendicular to the sound propagation direction. The velocity change as a function of the time is well approximated by a simple exponential form $(V_t - V_0)/V_0 = 0.0025(1 - e^{t/20.1})$. Cholesteric materials are very viscous and the magnetic anisotropy is very small. This is clearly demonstrated in Fig. 26 and is in contrast to the case of nematics, where equilibrium is reached almost instantaneously. If the rearrangement of the molecules is driven solely by the magnetic torque acting against the viscosity, the time constant of the above exponential form should be the same; however, the rotation of the field is performed for a given temperature. Furthermore, the velocity should approach the same value after a long enough time, whatever the previous field orientation may have been. In reality, however, the time constant varies from 10 to 30 min and the velocity anisotropy has a hysteresis. This is shown in Fig. 27(a). The data were taken at 56.2 °C. The field was rotated from 0° (the pitch axis is parallel to the sound propagation direction) to 90° and back to 0°, as the arrows indicate. In taking these data as long as $6\frac{1}{2}$ h elapsed at a given field orientation. After about 100 min following the field rotation no further significant change was noted. Nevertheless, the velocity measured in this manner depends on the way the field was rotated. The discrepancy is larger than the expected error introduced by the limited measuring time. The values at 0° and 90°, however, seem always to be much less history dependent. The nature of the data suggests that the helix axis prefers to stay perpendicular to the transducers or to the spacer wall; it is likely that once these configurations are realized they tend to be stable against rotation and the observed anisotropy probably results from only part of the sample rotating. This idea is further evidenced in Fig. 27(b), where, instead of applying the field at 0° or at 90°, it was first turned on at 60° and then rotated. Once the 90° orientation is realized the sample appears to stay that way. The same effect is seen for 0°.

Throughout, the measurements field was kept at 12.4 kG. A field of 6.5 kG had almost no effect; a higher field is obviously needed to overcome the boundary effects. The variable-path cell was designed to fit in a smaller pole gap (2 in.) and measurements at a higher field are planned. The temperature dependence of the velocity anisotropy is shown in Fig. 28. The transition temperature is

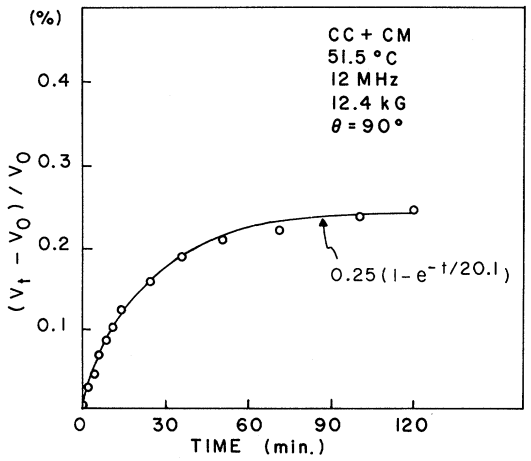

FIG. 26. Velocity change after the field was applied (at $t=0$) perpendicular to the sound propagation direction. A simple exponential form fits the data well.

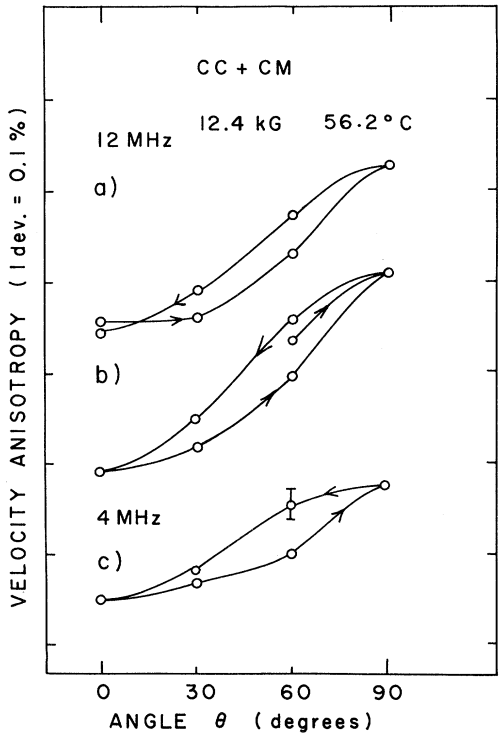

FIG. 27. Velocity anisotropy in a CC+CM mixture. The arrows indicate the way the magnetic field was rotated.

68 °C. In all cases the attenuation was constant within the error.

The hydrodynamic theory of Lubensky[2] predicts a small velocity anisotropy. The cause of the anisotropy, in spite of the similarity between cholesterics and nematics, can be found in the broken translational symmetry because of the twist of the director. More specifically, a deformation of the material in the direction of the pitch axis is different from that in a perpendicular direction, because the former includes change of pitch as well as volume change. The actual calculation is similar to that for the smectic-A phase, the pitch being analogous to the layer spacing of the smectic phase. A hydrodynamic theory is valid only when the wavelength of the excitation is much longer than the characteristic length of the system, which is the pitch in this case. Because the pitch is usually in the range of visible light (~5000 Å) the above condition is met only by ultrasonic experiments. The calculated anisotropy is, in our notation,

$$C_{33}-C_{11}=K_2'\left[\frac{q_0^2}{\rho}-2q_0\left(\frac{\partial q_0}{\partial \rho}\right)_{hs}\right], \tag{15}$$

where K_2' is an elastic constant associated with the bend deformation of the director $q_0=2\pi/\lambda_0$, λ_0 is the pitch, and h is a field conjugate to the change of λ_0 (analogous to ϕ_3). The derivative $(\partial q_0/\partial \rho)$ can be either positive or negative and its absolute value can possibly be large, in which case we could not determine the sign of Eq. (15); however, a reasonable guess is that the derivative is negligibly small. Typically $K_2'=10^{-6}$ dyn, $q_0=10^5$ cm^{-1}, and $\rho=1$ g/cm^3. These values yield $C_{33}-C_{11}=10^4$ (cm/sec)^2. C_{11} is about 10^{10} (cm/sec)^2; therefore the velocity anisotropy is $(C_{33}-C_{11})/(C_{11})^{1/2}=0.1$ cm/sec. The observed anisotropy is orders of magnitude larger and has the opposite sign.

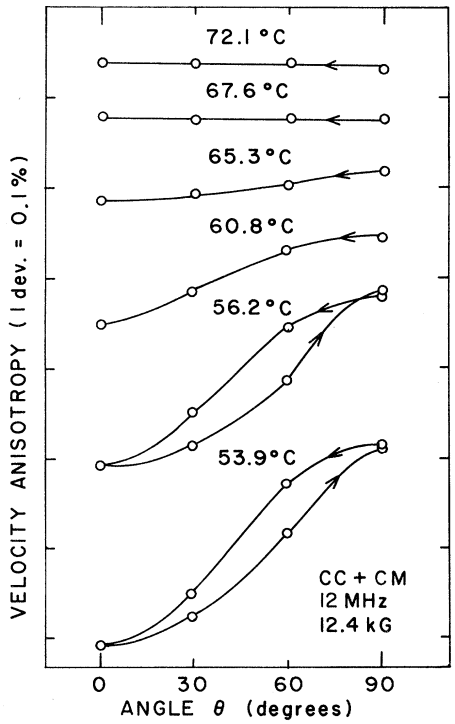

FIG. 28. Temperature dependence of the velocity anisotropy in a CC+CM mixture. The isotropic to cholesteric transition is at 68 °C.

The discrepancy is explained if one assumes that this is a dispersion effect similar to that observed in the nematics. In view of our model of cholesterics simply being twisted nematics, this is easily understood. When the sound propagates along the pitch axis, the director is always perpendicular to the wave vector. As was seen in the nematics (Fig. 7), this is the direction where the dispersive velocity is minimum. When the wave vector is perpendicular to the pitch axis, the angle between the director and the wave vector varies from 0° to 360° as a cycle of the spiral is progressed. Thus the velocity in this case should be larger, since the elastic constants both perpendicular and parallel to the director are sampled. A rough estimate, given in Appendix B and based on the dispersive velocity anisotropy in the nematics, shows a reasonable agreement as to the amount and sign of the measured anisotropy. If this is truly a dispersive effect the anisotropy should diminish as the sound frequency is lowered. Figure 27(c) shows typical data at 4 MHz. The anisotropy is decreased to about two-thirds of that at 12 MHz. Systematic measurements remain to be done to uncover the behavior in the zero-frequency limit.

APPENDIX A

Following the notations in Ref. 4 the rate of entropy production is written as

$$T\frac{d}{dt}(\rho s)=\frac{1}{T}\kappa_{ij}(\nabla_i T)(\nabla_j T)+\frac{2}{T}\sum_{\alpha}\xi_i^{\alpha}(\nabla_i T)(\nabla_j \phi_j^{\alpha})$$
$$+\eta_{ijkl}(\nabla_i v_j)(\nabla_l v_k)+\sum_{\alpha\beta}\Gamma^{\alpha\beta}(\nabla_i \phi_i^{\alpha})(\nabla_j \phi_j^{\beta}), \tag{A1}$$

where κ is the thermal conductivity, η is the viscosity, Γ is the mass diffusion constant (movement of mass relative to the ordered state), and ξ is the coupling constant between the mass diffusion and temperature gradient. The rate of change of the mechanical energy of the sound is then expressed as[12]

$$\dot{E}_{\text{mech}} = -T\dot{S} = -T\int \frac{d}{dt}(\rho s)\, d^3x \,. \tag{A2}$$

The sound attenuation constant is given by

$$\alpha = |\langle \dot{E}_{\text{mech}} \rangle| / 2V\langle E \rangle \,, \tag{A3}$$

where V is the sound velocity, E is the total energy of the sound, and the angular brackets indicate a time average. We consider a longitudinal wave in the 1-3 plane,

$$\begin{aligned} v_1 &= aq_1 \sin(\vec{q}\cdot\vec{r} - \omega t) \,, \\ v_2 &= 0 \,, \\ v_3 &= aq_3 \sin(\vec{q}\cdot\vec{r} - \omega t) \,, \end{aligned} \tag{A4}$$

where a is a constant. Then the calculation of the attenuation, although laborious, is very straightforward. We only show the final expressions for the smectic-A material for the attenuation due to the various contributions—the viscosity:

$$\frac{\omega^2}{2\rho V^3}\left[(\eta_2+\eta_4)\sin^4\theta + (2\eta_5+4\eta_3)\sin^2\theta\cos^2\theta + \eta_1\cos^4\theta\right]; \tag{A5}$$

the heat conduction;

$$\frac{\omega^2}{2\rho V^3}\,\frac{1}{TV^2}\,(\kappa_\perp \sin^2\theta + \kappa_\parallel \cos^2\theta)\left[\left(\frac{\partial T}{\partial \rho}\right)^2\rho^2 - 2\left(\frac{\partial T}{\partial \nabla_3 x}\right)\left(\frac{\partial T}{\partial \rho}\right)\rho\cos^2\theta + \left(\frac{\partial T}{\partial \nabla_3 x}\right)^2\cos^4\theta\right]; \tag{A6}$$

the diffusion:

$$\frac{\omega^2}{2\rho V^3}\,\frac{\zeta}{V^2}\cos^2\theta\left[\left(\frac{\partial \phi_3}{\partial \rho}\right)^2\rho^2 - 2\left(\frac{\partial \phi_3}{\partial \rho}\right)\left(\frac{\partial \phi_3}{\partial \nabla_3 x}\right)\rho\cos^2\theta + \left(\frac{\partial \phi_3}{\partial \nabla_3 x}\right)^2\cos^4\theta\right]; \tag{A7}$$

and the coupling term:

$$\frac{\omega^2}{2\rho V^3}\,\frac{2\xi}{TV^2}\cos^2\theta\left\{\left(\frac{\partial T}{\partial \rho}\right)\left(\frac{\partial \phi_3}{\partial \rho}\right)\rho^2 - \left[\left(\frac{\partial T}{\partial \nabla_3 x}\right)\left(\frac{\partial \phi_3}{\partial \rho}\right) + \left(\frac{\partial T}{\partial \rho}\right)\left(\frac{\partial \phi_3}{\partial \nabla_3 x}\right)\right]\rho\cos^2\theta + \left(\frac{\partial T}{\partial \nabla_3 x}\right)\left(\frac{\partial \phi_3}{\partial \nabla_3 x}\right)\cos^4\theta\right\} \,, \tag{A8}$$

where we chose s, ρ, and x as independent variables. Note that there are trigonometric functions of higher power than the fourth. Such terms do not exist in our simplified formula [Eqs. (6) and (7)]. Therefore the parametrization in Sec. II B is, strictly speaking, correct only when the viscosity is the dominant cause of the sound attenuation (which is usually the case).

APPENDIX B

We assume that, due to dispersion, a nematic phase has an elastic stiffness matrix, at a frequency ω, of the simple (block) form

$$\begin{bmatrix} C_{11} & C_{11} & C_{13} & \\ C_{11} & C_{11} & C_{13} & 0 \\ C_{13} & C_{13} & C_{33} & \\ & 0 & & 0 \end{bmatrix} \,. \tag{B1}$$

The cholesteric phase is realized when we twist the director, which coincides with the 3-axis, about the 2-axis. The new matrix (B1) twisted by an angle ϕ about the 2-axis is[32]

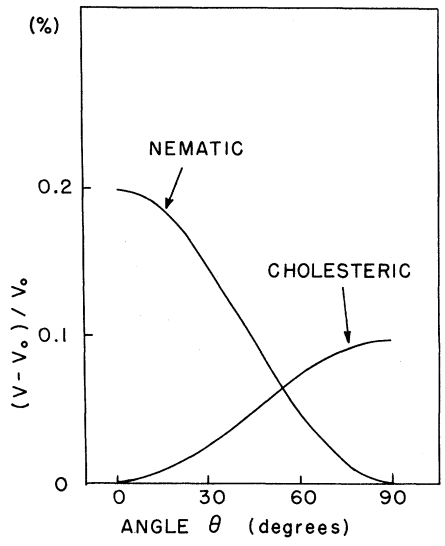

FIG. 29. Dispersive velocity anisotropy in a model nematic phase and in a cholesteric material made of the nematic by twisting the director along a pitch axis perpendicular to it. The angle θ is taken between the sound propagation direction and the pitch axis.

$$\begin{pmatrix} \cos^2\phi & 0 & \sin^2\phi \\ 0 & 1 & 0 \\ \sin^2\phi & 0 & \cos^2\phi \end{pmatrix} \begin{pmatrix} C_{11} & C_{11} & C_{13} \\ C_{11} & C_{11} & C_{13} \\ C_{13} & C_{13} & C_{33} \end{pmatrix} \begin{pmatrix} \cos^2\phi & 0 & \sin^2\phi \\ 0 & 1 & 0 \\ \sin^2\phi & 0 & \cos^2\phi \end{pmatrix} , \tag{B2}$$

where only the upper left 3×3 matrix is shown. Averaging over ϕ we have a new matrix

$$\frac{1}{8} \begin{pmatrix} 3C_{11}+2C_{13}+3C_{33} & 4C_{11}+4C_{13} & C_{11}+6C_{13}+C_{33} \\ 4C_{11}+4C_{13} & 8C_{11} & 4C_{11}+4C_{13} \\ C_{11}+6C_{13}+C_{33} & 4C_{11}+4C_{13} & 3C_{11}+2C_{13}+3C_{33} \end{pmatrix} .$$

The pitch axis is in the 2-direction. If the sound propagation direction θ is measured from the pitch axis, as was done in Sec. IV E, the velocity anisotropy is given by Eq. (4) with $\overline{C}_{11} = \frac{1}{8}(3C_{11}+2C_{13}+3C_{33})$, $\overline{C}_{13} = \frac{1}{2}(C_{11}+C_{13})$, $\overline{C}_{33} = C_{11}$, and $\overline{C}_{44} = 0$. We assume that $C_{11}C_{33} = C_{13}^2$, which means that the velocity anisotropy has a simple form, $V^2(\theta) = C_{11} + (C_{33} - C_{11})\cos^2\theta$; this form is a good approximation to our data on nematics. In nematics the anisotropy is typically $(C_{33} - C_{11})/C_{11} \cong 0.4\%$ at 12 MHz. Then a cholesteric phase made of this nematic and twisted along the pitch axis has an anisotropy $(\overline{C}_{33} - \overline{C}_{11})/\overline{C}_{11} \cong -0.2\%$. Both curves, the anisotropy of the velocity in a nematic phase and that in a corresponding cholesteric phase, are shown in Fig. 29, which compares well with Fig. 27.

ACKNOWLEDGMENT

We would like to thank C. W. Woo for discussions.

---

*Work supported by the U. S. Atomic Energy Commission, the Northwestern University Materials Research Center, and the National Science Foundation Grant No. DMR 74-09661.

†Present address: Department of Physics, University of California, Berkeley, Calif. 94720.

[1]See, for instance, J. L. Ericksen, Arch. Rational Mech. Anal. 4, 231 (1960); F. M. Leslie, Quart. J. Mech. Appl. Math. 19, 357 (1966).

[2]T. C. Lubensky, Phys. Rev. A 6, 452 (1972).

[3]D. Forster, T. C. Lubensky, P. C. Martin, J. Swift, and P. S. Pershan, Phys. Rev. Lett. 26, 1016 (1971), and the references therein.

[4]P. C. Martin, O. Parodi, and P. S. Pershan, Phys. Rev. A 6, 2401 (1972).

[5]D. Forster, Ann. Phys. (N.Y.) 85, 505 (1974).

[6]P. G. de Gennes, Solid State Commun. 10, 753 (1972).

[7]See, for instance, M. E. Mullen, B. Lüthi, and M. J. Stephen, Phys. Rev. Lett. 28, 799 (1972); K. A. Kemp and S. V. Letcher, *ibid.* 27, 1634 (1971); A. E. Lord and M. M. Labes, *ibid.* 25, 570 (1970).

[8]A. E. Lord, Phys. Rev. Lett. 29, 1366 (1972).

[9]K. Miyano and J. B. Ketterson, Phys. Rev. Lett. 31, 1047 (1973).

[10]See, for instance, H. B. Huntington, in *Solid State Physics*, edited by F. Seitz and D. Turnbull (Academic, New York, 1958), Vol. 7.

[11]S. M. Rytov, Zh. Eksp. Teor. Fiz. 33, 166 (1957) [Sov. Phys.—JETP 6, 130 (1958)].

[12]L. D. Landau and E. M. Lifshitz, *Fluid Mechanics* (Pergamon, London, 1959).

[13]The dispersion in a nematic liquid crystal was analyzed by F. Jähnig [Z. Phys. 258, 199 (1973)]. The data did not quite behave as expected, possibly because they were gathered from many sources where the experimental conditions, especially the impurity content, may differ widely. It is thus important to measure the frequency dependence of the velocity and attenuation at the same time.

[14]W. Schaaffs, in *Landolt-Börnstein* (Springer, Berlin, 1967), New Series, Group II, Vol. 5.

[15]B. M. Abraham, Y. Eckstein, J. B. Ketterson, and J. Vignos, Cryogenics 9, 274 (1969).

[16]W. L. McMillan, Phys. Rev. A 7, 1419 (1973).

[17]For instance, L. Cheung, R. B. Meyer, and H. Gruler, Phys. Rev. Lett. 31, 349 (1973); M. Delaye, R. Ribotta, and G. Durand, *ibid.* 31, 443 (1973); B. Cabane and W. G. Clark, Solid State Commun. 13, 129 (1973).

[18]S. Torza and P. E. Cladis, Phys. Rev. Lett. 32, 1406 (1974).

[19]P. E. Cladis, Phys. Rev. Lett. 31, 1200 (1973).

[20]W. J. Lin, P. H. Keyes, and W. B. Daniels (unpublished).

[21]K. A. Kemp and S. V. Letcher, Phys. Rev. Lett. 27, 1634 (1971).

[22]Y. Liao, N. A. Clark, and P. S. Pershan, Phys. Rev. Lett. 30, 639 (1973).

[23]D. Demus and H. Sackmann, Z. Phys. Chem. 222, 127 (1963).

[24]Z. Luz and S. Meiboom, J. Chem. Phys. 59, 275 (1973).

[25]J. W. Doane, R. S. Parker, B. Cvikl, D. L. Johnson, and D. L. Fishel, Phys. Rev. Lett. 28, 1694 (1972).

[26]V. S. V. Rajan and J. J. C. Picot, Mol. Cryst. Liq. Cryst. 20, 55 (1973).

[27]H. Arnold, Z. Phys. Chem. 226, 146 (1965).

[28]L. D. Landau and E. M. Lifshitz, *Theory of Elasticity* (Pergamon, London, 1970).

[29]T. R. Taylor, J. L. Fergason, and S. L. Arora, Phys. Rev. Lett. 24, 359 (1970).
[30]R. A. Wise, D. H. Smith, and J. W. Doane, Phys. Rev. A 7, 1366 (1973).
[31]E. Sackmann, S. Meiboom, L. C. Snyder, A. E. Meixner, and R. E. Dietz, J. Am. Chem. Soc. 90, 3567 (1968).
[32]See, for instance, A. V. Hershey, J. Appl. Mech. 21, 236 (1954).